HHS Public Access

Author manuscript

Neurobiol Dis. Author manuscript; available in PMC 2016 December 01.

Published in final edited form as:

Neurobiol Dis. 2015 December ; 84: 109–119. doi:10.1016/j.nbd.2015.06.013.

Oxidative stress and lipid peroxidation are upstream of amyloid pathology

Muriel Arimon[1], **Shuko Takeda**, **Kathryn L. Post**[2], **Sarah Svirsky**, **Bradley T. Hyman**, and **Oksana Berezovska**[†]

MassGeneral Institute for Neurodegenerative Disease, Department of Neurology, Massachusetts General Hospital, Harvard Medical School, CNY 114, 16th Street, Charlestown 02129, Massachusetts, USA

Abstract

Oxidative stress is a common feature of the aging process and of many neurodegenerative disorders, including Alzheimer's disease. Understanding the direct causative relationship between oxidative stress and amyloid pathology, and determining the underlying molecular mechanisms is crucial for the development of more effective therapeutics for the disease. By employing microdialysis technique, we report local increase in the amyloid-$\beta_4$2 levels and elevated amyloid-$\beta_4$2/40 ratio in the interstitial fluid within 6h of direct infusion of oxidizing agents into the hippocampus of living and awake wild type mice. The increase in the amyloid-$\beta_4$2/40 ratio correlated with the pathogenic conformational change of the amyloid precursor protein-cleaving enzyme, presenilin1/γ-secretase. Furthermore, we found that the product of lipid peroxidation 4-hydroxynonenal, binds to both nicastrin and BACE, differentially affecting γ- and β-secretase activity, respectively. The present study demonstrates a direct cause-and-effect correlation between oxidative stress and altered amyloid-β production, and provides a molecular mechanism by which naturally occurring product of lipid peroxidation may trigger generation of toxic amyloid-β_{42} species.

Graphical abstract

[†]To whom correspondence should be addressed: Oksana Berezovska, MassGeneral Institute for Neurodegenerative Disease (MIND), Massachusetts General Hospital, Harvard Medical School, 114 16th Street, Charlestown, MA 02129, USA, Phone: 617-726-7478, Fax: 617-724-1480, OBerezovska@partners.org.

[1]Current Addresses:
Institut de Neurociències, Department de Bioquímica i Biologia Molecular, Universitat Autònoma de Barcelona, 08193 Bellaterra, Spain

[2]Brain Research Center, University of British Columbia, Vancouver, BC V6T2B5, Canada

Author contributions: M.A. and O.B. designed the experiments, M.A., S.T., K.L.P., and S.S. performed experiments and analyzed the data; M.A. and O.B. wrote the manuscript. O.B., M.A., S.T., and B.T.H. discussed the results, provided constructive criticism of the findings, and commented on the manuscript.

Conflict of interest: The authors declare that they have no conflict of interest.

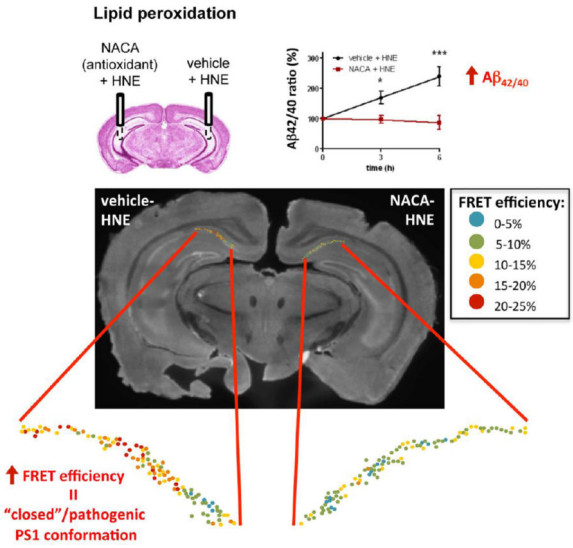

Keywords

Oxidative stress; lipid peroxidation; Alzheimer's disease; microdialysis; amyloid beta; β-secretase; presenilin; 4-hydroxynonenal

Introduction

Alzheimer's disease (AD) is an age-related neurodegenerative disorder characterized clinically by progressive memory loss and cognitive decline. The major neuropathological hallmarks of AD are neuronal and synapse loss, accumulation of intraneuronal fibrillary tangles, and deposition of extracellular amyloid plaques consisting of amyloid-β peptide (Aβ) (Hardy and Selkoe 2002). Aβ generation is mediated by sequential cleavage of the amyloid precursor protein (APP) by β-secretase (BACE) and γ-secretase. The latter is an enzymatic complex composed of presenilin (PS1 or PS2), nicastrin (NCT), Aph-1 and presenilin enhancer-2 (Pen2) (Bergmans and De Strooper 2010). Familial early-onset AD (FAD) is caused by autosomal dominant mutations in presenilin (*PSEN1* and *PSEN2*) and APP genes. However, the sporadic late onset form of AD (SAD) represents the vast majority of the cases, and yet its etiology remains poorly understood. The major non-genetic risk factor involved in the pathogenesis of SAD is aging, which is often accompanied by accumulation of reactive oxygen species (ROS) (Finkel and Holbrook 2000). ROS are generated as a result of normal intracellular metabolism and may function as signaling molecules (Nemoto, Takeda et al. 2000; Nishikawa, Edelstein et al. 2000). At the same time, a number of external agents such as ultraviolet light or environmental toxins, or internal inflammatory processes can trigger excessive ROS production (Finkel and Holbrook 2000). An imbalance due to either increased ROS production or decreased antioxidant defense mechanisms leads to oxidative stress, which damages various cell components via modification of proteins, lipids and DNA, and disrupts numerous cellular processes.

Oxidative damage can be observed in the brain of patients with mild cognitive impairment (MCI)(Lovell and Markesbery 2001; Butterfield, Reed et al. 2006), a transition stage

between normal aging and dementia, and is detected at the early stages of AD (Mangialasche, Polidori et al. 2009; Reed, Pierce et al. 2009; Reed, Pierce et al. 2009; Sultana and Butterfield 2010; Sun 2010; Subramanian, Tam et al. 2011). It has been reported that the level of antioxidant enzymes is diminished, whereas inflammation, ROS production, and the level of oxidative stress markers are elevated in the brain of AD patients, compared to that in the age-matched controls (Sultana and Butterfield 2010; Krstic and Knuesel 2013). Specifically, 4-hydroxynonenal (HNE), an aldehyde product of lipid peroxidation, has been shown to accumulate in the brain due to normal aging, and is present at high levels and believed to be associated with amyloid pathology in MCI and AD patients (Sajdel-Sulkowska and Marotta 1984; Butterfield, Hensley et al. 1997; Butterfield, Reed et al. 2006; Shichiri, Yoshida et al. 2011; Subramanian, Tam et al. 2011; Chavez-Gutierrez, Bammens et al. 2012). Interestingly, lipid peroxidation can be detected prior to Aβ deposition in a mouse model of AD (Pratico, Uryu et al. 2001), suggesting that it may be upstream of Aβ pathology. On the other hand, increased oxidative stress has been found in the vicinity of amyloid plaques (McLellan, Kajdasz et al. 2003; Garcia-Alloza, Dodwell et al. 2006; Xie, Hou et al. 2013) and Aβ peptide itself has been shown to trigger increase in oxidative stress (Harris, Hensley et al. 1995; Butterfield 2002; Butterfield, Griffin et al. 2002; Atamna and Boyle 2006; Cai, Zhao et al. 2011). However, the causality and interrelationship between oxidative stress and Aβ pathology remains poorly understood.

To determine whether oxidative stress may be an initiator of Aβ pathology, we employed *in vivo* microdialysis to locally induce acute oxidative stress in the brain of living mice. We provide evidence of a direct causative role of oxidative stress, and specifically lipid peroxidation, in promoting Aβ42 production and increasing the Aβ42/40 ratio in the brain of wild type mice. We report that HNE covalently modifies nicastrin (NCT) in the γ-secretase complex as well as BACE, via the formation of HNE adducts. These covalent modifications result in altered γ- and β-secretase activities, and cause pathogenic conformational change in PS1/γ-secretase associated with altered APP processing.

Materials and Methods

In vivo microdialysis

In vivo microdialysis sampling of brain interstitial Aβ was performed as described previously (Wolfe 2007; Takeda, Sato et al. 2011). The microdialysis probes used had a 4 mm shaft with a 3.0 mm, 1000 kDa molecular weight cutoff (MWCO) polyethylene (PE) membrane (PEP-4-03, Eicom, Kyoto, Japan). Before use, the probe was conditioned by briefly dipping it in ethanol, and then washed with sterile artificial cerebrospinal fluid (ACSF) perfusion buffer (122 mM NaCl, 1.3 mM $CaCl_2$, 1.2 mM $MgCl_2$, 3.0 mM KH_2PO_4, 25.0 mM $NaHCO_3$). The preconditioned probe's outlet and inlet were connected to a peristaltic pump (ERP-10, Eicom, Kyoto, Japan) and a microsyringe pump (ESP-32, Eicom, Kyoto, Japan), respectively, using fluorinated ethylene propylene (FEP) tubing (ϕ 250 μm i.d.). Probe implantation was performed as previously described (Cirrito, May et al. 2003; Takeda, Sato et al. 2011), with slight modifications. Briefly, the animals were anesthetized with isoflurane, while a guide cannula (PEG-4, Eicom, Kyoto, Japan) was stereotactically implanted in both hippocampi (bregma −3.1 mm, 2.8 mm lateral to midline, −1.2 mm

ventral to dura). The guide was fixed using binary dental cement. Three days after guide cannula implantation, the mice were placed in a standard microdialysis cage and a probe was inserted through the guide. After insertion of the probe, in order to obtain stable baseline recordings, the probe and connecting tubes were perfused with ACSF for 180 min at a flow rate of 10 μl/min before baseline sample collection. First, a baseline sample was collected for 180 min before the delivery of either 3 mM 4,4'-dithiodipyridine (DTDP) (Sigma-Aldrich) or 5 mM 4-hydroxynonenal (HNE) (Cayman Chemical, Ann Arbor, MI) in the right hemisphere, or vehicle EtOH as a control in the left hemisphere. Samples were collected from the brain of mice at 180 min intervals at a flow rate of 0.5 μl/min. The antioxidant N-acetylcysteine amide (NACA) (Sigma-Aldrich) diluted in DMSO was delivered at 7.5 mM for 12 hours prior to the oxidative stress. During microdialysis sample collection, mice were awake and freely moving in the microdialysis cage designed to allow unrestricted movement of the animals without applying pressure on the probe assembly (AtmosLM microdialysis system, Eicom, Kyoto, Japan).

Aβ quantification

Aβ40 and Aβ42 concentrations were determined by Human/Rat β Amyloid (40 or 42) sandwich ELISA (Wako Pure Chemicals Industries, Osaka, Japan), according to the manufacturer's instructions. To dissociate oligomerized Aβ, samples were incubated with 500 mM guanidine HCl for 30 min at room temperature.

Immunohistochemistry

Following the microdialysis, mouse brains were removed and post-fixed in 4% paraformaldehyde (PFA) solution for 72 hours, cryoprotected in 30% sucrose, 30% (v/v) ethylene glycol in 0.1M PBS and sectioned on a freezing microtome at 35 um thickness. The free-floating brain tissue sections were washed with PBS and permeabilized in blocking buffer (1.5% Normal Donkey Serum, 0.4% Triton-X100 in PBS) for 60 minutes. Samples were then incubated overnight at 4°C with the respective primary antibodies (goat PS1-N-Terminus (NT), Millipore; rabbit PS1-C-Terminus (CT), Sigma-Aldrich) in blocking buffer (1.5% Normal Donkey Serum, 0.1% Triton-X100 in PBS). Alexa488- and Cy3-conjugated secondary antibodies (donkey-anti-goat AlexaFluor488, Invitrogen; donkey-anti-rabbit Cy3, Jackson ImmunoResearch) were used for detection. Sections were coverslipped with Vectashield mounting medium without DAPI (Vector Laboratories), sealed, and stored at 4°C until imaged.

Fluorescence Lifetime Imaging Microscopy (FLIM)

The relative proximity between fluorescently labeled PS1 N- and C-termini, as a measure of PS1 conformation, was monitored using Fluorescence Lifetime Imaging microscopy (FLIM), as previously described (Lleo, Berezovska et al. 2004; Berezovska, Lleo et al. 2005). Briefly, mouse brain sections immunostained with Alexa488 (A488) as the donor fluorophore to label PS1 NT and Cy3 as the acceptor fluorophore to label PS1 CT (see above) were imaged on the LSM510 Zeiss microscope equipped with Becker & Hickl (Berlin, Germany) hardware and software. Donor fluorophore lifetimes were measured using multi-exponential analysis to distinguish between PS1 molecules in different conformational states as described in detail previously (Wahlster, Arimon et al. 2013).

TheFluorescence Resonance Energy Transfer efficiency (%E_{FRET}) reflecting PS1 NT-CT proximity was calculated as the percent of decrease in the baseline lifetime of the A488 donor fluorophore due to presence of the Cy3-acceptor fluorophore in close proximity using the following equation:

$$\%E_{FRET} = 100^{*}(t1 - t2)/t1$$

where t1 is the lifetime of the A488 donor fluorophore alone (FRET absent), and t2 is the A488 lifetime in the presence of Cy3 (FRET present). The FRET efficiency values could be color-coded to show distribution of neurons with PS1 in different conformational states within the CA1 area of hippocampus after the treatment. Yellow-to-red pixels represent high %E_{FRET} ("closed" PS1 conformation), whereas green-blue pixels represent low %E_{FRET} ("open" PS1 conformation).

Membrane-enriched fractions from mouse brains and cell free γ-secretase assay

Wild-type mouse brain tissue was homogenized in buffer A (50 mM MES pH 6.0, 150 mM KCl, 5 mM $MgCl_2$, 5 mM $CaCl_2$) containing complete protease inhibitor mixture (Roche) with a teflon homogenizer, and cell debris and nuclei were removed by centrifugation at 800 × *g* for 10 min. Supernatants were then centrifuged at 100,000 × *g* for 60 min, resulting pellets were resuspended in ice cold carbonate buffer (100 mM Na_2CO_3 pH 11.2), and the centrifugation was repeated. Pellets were resuspended in buffer B (50 mM Hepes pH 7.0, 150 mM KCl, 5 mM $MgCl_2$, 5 mM $CaCl_2$), and the centrifugation was repeated. Membrane enriched fractions were solubilized in buffer B + 1% CHAPSO for 60 min at 4°C, and centrifuged at 100,000 × *g* for 60 min. All procedures were performed at 4°C and the membranes suspensions were stored at −80°C. Resulting supernatants are referred to as membrane-enriched fractions. Membrane-enriched fractions (0.125 mg/ml) were incubated with human C100-Flag (1 uM) in buffer B containing 0.25% CHAPSO at 37 °C for 4 h. Negative controls were incubated either at 4°C or at 37 °C with the γ-secretase inhibitor (GSI) L-685,458 (50 nM, Calbiochem). Reaction was stopped by placing the samples in ice.

Cell lines and primary neuronal cultures

HEK293 cells were transfected with C99-flag construct (Uemura, Farner et al. 2010) using Lipofectamine 2000 reagent (Life Technologies) and were treated 24h post-transfection. GFP plasmid was co-transfected along as a control for transfection efficiency.

Primary neuronal cultures were obtained from cerebral cortex of mouse embryos at gestation day 14–16 (Charles River Laboratories, Wilmington, MA), as described previously (Berezovska, Frosch et al. 1999). Briefly, the dissected tissue was dissociated by trypsinization for 5 minutes and re-suspended in neurobasal medium (Gibco, Invitrogen, Gaithersburg, MD) supplemented with 10% fetal bovine serum (Gibco, Invitrogen), 2 mM/L L-glutamine (Gibco, Invitrogen), 100 U/mL penicillin and 100 μg/mL streptomycin (Gibco, Invitrogen). Neurons were plated in 35-mm glass bottom culture dishes (MatTek Corporation, Ashland, MA) previously coated with Poly-D-lysine hydrobromide at 100 μg/ml (Sigma-Aldrich, St. Louis, MO) and cultures were maintained at 37 °C with 5% CO_2. Media was changed after 2h to neurobasal medium supplemented with 2% B27 (Gibco,

Invitrogen), 2 mM L-glutamine, penicillin and streptomycin. Neurons were cultured for 7–14 days *in vitro* before the treatment.

In vitro drug treatment

To induce oxidative stress, primary neurons were treated with either 100 μM DTDP or 1 mM HNE (both diluted in ethanol) for 20 min or 3 h. γ-secretase inhibitor DAPT (Sigma) was used overnight at 1 μM concentration.

Immunoprecipitation and immunoblotting

For immunoprecipitation, primary neurons were washed with ice-cold PBS and were collected in lysis buffer (50 mM HEPES pH 7.4, 100 mM NaCl, 0.1 mM EDTA, 1% (w/v) CHAPSO) containing complete protease inhibitor mixture (Roche). Samples were passed through a 27G needle and incubated 1h at 4°C to completely solubilize membranes. After centrifugation at 20,000 × g for 20 min, protein concentration was determined in the resultant supernatant (solubilized membranes). Samples were pre-cleared with 20 μl of protein-G Sepharose beads (Invitrogen) for 2 h at 4°C. After removing the beads by centrifugation, supernatants were incubated with anti-PS1-NT (Millipore #AB1575) and anti-PS1-loop (Millipore #MAB5232) antibodies, or control IgGs (normal goat and mouse serum, Jakson ImmunoResearch) for 12/24 h at 4°C. Next day, protein-G Sepharose beads were added to the samples for 1–2 h. After several washes with lysis buffer, immunoprecipitated samples were eluted by incubation with sample buffer for 10 min at 95°C, and applied to SDS-polyacrylamide gels.

For Western blotting, cells were washed with ice-cold PBS and then were incubated with lysis buffer (50 mM HEPES pH 7.4, 100 mM NaCl, 0.1 mM EDTA, 1% Triton-X 100) containing complete protease inhibitor mixture (Roche). Cells were sonicated and centrifuged at 20,000 × g for 20 min at 4°C before determining protein concentration.

Samples were incubated with sample buffer for 5 min at 95°C, applied to SDS-polyacrylamide gels (SDS-PAGE) and transferred to nitrocellulose membranes (0.1 um - 0.2 um pore size, Whatman). Membranes were probed with the following antibodies: anti-FLAG (1:2000, Wako), GFP (1:2000, Abcam), actin (1:2000, Abcam), nicastrin (1:1000, Sigma), HNE (1:500, Abcam), BACE (1:1000, Cell Signaling), 6E10 (1:1000, Covance), anti-mouse/rat APP (597) (corresponding to Aβ 1–16) (1:100, IBL). Either horseradish peroxidase (HRP)-conjugated (1:2000, Bio-Rad) or infrared (IR)-dye conjugated (1:7500, IRDye680 or 800, Li-Cor Biosciences) secondary antibodies were used. Quantification of band density was determined by densitometric analysis in ImageJ software (National Institutes of Health).

Statistical analysis

Statistical analyses were performed using Graph Pad Prism software (GraphPad Software Inc., La Jolla, CA). Data is expressed as mean ± SEM. D'Agostino & Pearson omnibus normality test was used to evaluate the normality of the distributions of values. Two-sided Student's t-test was used for 2-group comparisons. The microdialysis data were analyzed using two-way ANOVA with repeated measures and Bonferroni post-test. Values were

considered significant at *p < 0.05. Higher significance is indicated as follows: **p < 0.01, ***p < 0.001.

Results

Locally induced oxidative stress in vivo triggers local increase in Aβ42 levels and Aβ42/40 ratio

To determine the effect of oxidative stress on Aβ, we locally delivered oxidizing agents into the brain of living and awake mice using microdialysis technique. The levels of Aβ40 and Aβ42 were concomitantly quantified in the collected interstitial fluid (ISF). Two microdialysis probes were surgically implanted into the brain of ~12 months old wild-type mice, one probe into each hemisphere targeted to hippocampus (Fig. 1A). One probe was used to deliver the oxidizing agent (right hemisphere), and the contralateral side (left hemisphere) received infusion of the vehicle control. Two different compounds were used: 4,4'-dithiodipyridine (DTDP), a strong cell-permeant thiol-reactive agent inducing oxidative stress, and 4-hydroxynonenal (HNE), a naturally occurring aldehyde by-product of lipid peroxidation (see Supplementary Fig. 4 for detailed chemical structure). We used 3 mM DTDP and 5 mM HNE for *in vivo* infusion since it is estimated that only around 10–15% of the drug is delivered across the microdialysis probe membrane into ISF at the 0.5 ul/min flow rate (Takeda, Sato et al. 2011), and is diluted further as it diffuses through the interstitial fluid. After establishing a baseline of Aβ levels for each individual animal/hemisphere (see Materials and Methods), DTDP or HNE diluted in artificial cerebrospinal fluid (ACSF) were delivered into the brain, and ISF samples were collected after 3h and 6h of infusion for Aβ ELISA quantification (Fig. 1A).

A significant increase in the levels of both Aβ40 and Aβ42 was observed after 3h and 6h of DTDP treatment, with an increase in the Aβ42/40 ratio as compared to the vehicle-treated contralateral hemisphere (Fig. 1B). Treatment with HNE triggered an increase in the Aβ42 levels only, with no significant changes in the Aβ40, leading to an even higher increase in the Aβ42/40 ratio (Fig. 1C).

Increased susceptibility to oxidative stress are known to occur during aging (Finkel and Holbrook 2000). Therefore, we next compared the extent of the effect of strong oxidant DTDP on Aβ42 levels in 4-month old (young) and compared them to that in 12 month-old (old) mice. We found that after 3h of treatment, young animals displayed the same increase in the Aβ40 and Aβ42 levels as the old animals (Fig. 2 vs Fig. 1B). However, a significant recovery of both Aβ40 and Aβ42 levels was observed in young animals after 6h of DTDP treatment, with the level of Aβ42 returning to that of the vehicle-treated hemisphere, which was not the case for old animals. Of note, young animals did not exhibit any change in the Aβ42/40 ratio after either 3h or 6h of DTDP treatment (Fig. 2). These data indicate that young animals are more resilient to the acute oxidative stress insults, which old animals are not able to overcome.

Oxidative stress and lipid peroxidation induce a change in PS1 conformation

We have previously established that changes in the Aβ42/40 ratio closely correlate with changes in the conformation of PS1 in cells *in vitro* (Berezovska, Lleo et al. 2005; Uemura, Lill et al. 2009). Here, we assessed whether the observed increase in the Aβ42/40 ratio in mouse ISF induced by DTDP and HNE treatment *in vivo* was associated with a similar change in PS1 conformation. The brain sections of mice used for the microdialysis were immunostained with PS1 antibodies to fluorescently label the N-terminus (NT) and C-terminus (CT) of PS1. *Ex vivo* tissue fluorescent lifetime microscopy (FLIM) was performed to determine the relative proximity between PS1-NT and -CT (PS1 conformation), which we expressed as FRET efficiency, $\%E_{FRET}$, (see Methods) in individual neurons of the CA1 region of the hippocampus. We found that both DTDP and HNE significantly increase the mean $\%E_{FRET}$ values in the neurons of CA1 area compared to the vehicle treatment (Fig. 3A). This suggests that oxidative stress triggers pathogenic, “closed”, conformational change in PS1 molecules, which in turn relates to the observed increase in Ab42/40 ratio (Fig. 1C). To show the distribution of neurons with PS1 in predominantly “closed” or “open” conformations, the mean $\%E_{FRET}$ for each individual neuron was color-coded and mapped over the CA1 area analyzed by FLIM. Fig. 3B shows a higher number of neurons with pathogenic “closed” PS1 conformation (higher $\%E_{FRET}$, color-coded in yellow-red) in the hemisphere where oxidative stress was induced.

To assess possible glia activation after the oxidative stress induction, the same brains treated with HNE or DTDP by microdialysis were immunostained with astrocytic (GFAP) and microglial (Iba1) markers. We did not observe any significant increase in the GFAP or Iba1 levels in the HNE treated hemispheres after 6h treatment (Supplementary Fig. 1). However, a significant increase in the GFAP immunoreactivity was detected in the DTDP treated hemispheres (Supplementary Fig.1), suggesting an astrocytic response to this compound.

Antioxidant NACA prevents HNE-induced changes in Aβ levels and in PS1 conformation

To confirm that the observed changes in the ISF Aβ42 levels are produced by oxidative stress, the antioxidant N-acetylcysteine amide (NACA) (7.5 mM) was delivered to the brain via microdialysis prior to the administration of HNE (Fig. 4A). This pretreatment with NACA completely abolished the effect of HNE on Aβ42 levels (Fig. 4B), whereas pretreatment with the vehicle had no effect, demonstrating that oxidative stress is the major culprit for observed increase in the Aβ42 level and the Aβ42/40 ratio. It should be noted that HNE itself is not a free radical but rather a product of arachidonic acid oxidation, an α,β-unsaturated hydroxyalkenal, that is significantly elevated during oxidative stress. The free thiol of NACA binds to HNE by Michael addition, preventing the reaction of HNE with proteins that affects their structure and function (Subramaniam, Roediger et al. 1997; Sun 2010). Therefore, antioxidants containing thiols, such as NACA, are the most effective in protecting against HNE damage.

Since antioxidant treatment was able to halt increase of the Aβ42/40 ratio, we next examined whether NACA would also prevent HNE-induced changes in the PS1 conformation. Indeed, the mean FRET efficiency found in the NACA-HNE treated hemisphere was significantly lower compared to the vehicle-HNE treated hemisphere (Fig. 4 C–D, color-coded in blue-

green), suggesting that antioxidant NACA is able to prevent HNE-induced “closed” pathogenic conformational change of PS1.

HNE treatment inhibits γ-secretase activity

To better understand the mechanism(s) by which oxidative stress affects PS1 and Aβ levels, we next evaluated whether DTDP and HNE may have a direct effect on γ-secretase. First, we monitored the expression level of γ-secretase components in mouse primary neurons treated with DTDP or HNE, and did not find significant changes in the PS1, NCT or Pen2 protein expression levels due to oxidative stress (data not shown). Furthermore, neither DTDP nor HNE affected the mobility of the γ-secretase complex to migrate on a native gel (Supplementary Fig. 2), suggesting that there is no drastic structural alteration of the complex.

Next, we assessed whether DTDP or HNE affect activity of the γ-secretase using membrane-enriched fractions purified from wild-type mouse brains. To bypass the effect of BACE, membrane-enriched fractions were incubated with equal amounts of human APP C100-flag peptide, an immediate substrate of the γ-secretase, and treated with DTDP, HNE or vehicle control for 4h. Aβ measurements show that the HNE treatment triggers a drastic decrease in the level of both Aβ40 and Aβ42, similar to that achieved by treatment with the γ-secretase inhibitor (GSI) L-685,458, or by incubation at 4°C (negative controls) (Fig. 5A). In contrast, DTDP did not significantly alter the levels of Aβ40 and Aβ42 in the cell-free γ-secretase activity assay.

To further evaluate the effect of oxidative stress on γ-secretase activity, a flag-tagged APP C99 fragment (C99-flag) was transiently transfected into HEK293 cells prior to treatment with either DTDP or HNE. Consistent with the findings in the cell-free assay, we found that HNE causes significant accumulation of the C99-flag (Fig. 5B) as compared to the vehicle control, further supporting our finding of impaired γ-secretase activity by HNE. There was no statistically significant effect of DTDP on the C99-flag levels after 3h of the treatment.

To determine whether HNE exerts its effect on γ-secretase via direct modification of the complex, γ-secretase was immunoprecipitated from DTDP or HNE treated neurons, and the eluates were probed for HNE adducts. No HNE adducts were found on PS1, the catalytic subunit of the complex, or Pen2. However, a significant increase in the HNE adducts levels was detected on nicastrin (NCT) (Fig. 6). These data suggest that NCT modification by HNE could affect γ-secretase activity.

Effect of HNE and DTDP on β-secretase

Next we examined whether BACE level or activity were affected by DTDP or HNE. Treatment of primary neurons with DTDP or HNE showed no significant difference in the BACE level as compared to that in the vehicle treated cells (Fig. 7A). To evaluate BACE activity independently of γ-secretase, primary neurons were pretreated overnight with the γ-secretase inhibitor DAPT and the level of endogenous APP C99 fragments was compared between vehicle and DTDP or HNE treated samples. The APP C99 level was significantly elevated in the DAPT+HNE treated cells, compared to the DAPT+vehicle controls (Fig.

7B), suggesting an increase in the BACE activity triggered by HNE. No difference in C99 levels was observed after the DTDP treatment.

Interestingly, we found that BACE is also directly modified by HNE, as determined by significantly higher amount of the HNE adducts on BACE immunoprecipitated from primary neurons treated with HNE, compared to that in DTDP or vehicle treated cells (Fig. 8). This suggests that covalent modification of BACE by HNE adducts may lead to the abnormal increase in its enzymatic activity.

Discussion

To determine the relationship between oxidative stress and Aβ pathology, and to establish whether oxidative stress, and specifically lipid peroxidation, may be an initiator of Aβ pathology, we employed *in vivo* microdialysis to locally induce acute oxidative stress in the brains of awake mice using a naturally occurring product of lipid peroxidation, HNE (Sayre, Zelasko et al. 1997; Cutler, Kelly et al. 2004; Williams, Lynn et al. 2006), and a strong thiol-reactive agent, DTDP. Our results show that both compounds alter the ISF levels of Aβ within 3–6h of treatment. Importantly, both HNE and DTDP significantly increased the level of highly fibrillogenic Aβ species, Aβ42, and resulted in elevated Aβ42/40 ratio *in vivo*. The Aβ42/40 ratio, rather than total absolute Aβ levels, has been reported to play a crucial role in Aβ deposition and neurodegeneration (Borchelt, Thinakaran et al. 1996; Lewczuk, Esselmann et al. 2004; Wiltfang, Esselmann et al. 2007; Wolfe 2007; Kuperstein, Broersen et al. 2010). It has been previously shown that the Aβ42/40 ratio strongly correlates with the conformation of PS1/γ-secretase in cells *in vitro* (Lleo, Berezovska et al. 2004; Berezovska, Lleo et al. 2005; Isoo, Sato et al. 2007; Serneels, Van Biervliet et al. 2009), proposing that pathogenic structural changes may affect the γ-secretase cleavage site. Indeed, in a recent study, we found that changes in conformation of endogenous PS1 do occur in normal aging in mouse brain and in sporadic AD patients (Wahlster, Arimon et al. 2013). Moreover, we observed more pronounced PS1 conformational changes in close proximity to amyloid plaques, suggesting a link between the microenvironment surrounding Aβ plaques, PS1 conformation and Aβ deposition in AD brain (Wahlster, Arimon et al. 2013). Concurring with these findings, here we detect a similar pathogenic “closed” PS1 configuration in the hippocampus of mice treated with the oxidative agents DTDP and HNE. This observation strongly supports the hypothesis that changes in conformation of PS1/γ-secretase, and consequent elevation in the Aβ42/40 ratio could be early events occurring due to local increase in the oxidative stress and its products in the brain. Indeed, pretreatment with antioxidant NACA prior to the HNE insult completely abolished HNE-triggered increase in the Aβ42 and Aβ42/40 ratio, as well as prevented change in the PS1 conformation, confirming the specificity of the observed effect. Along the same lines, we found that young mice were able to recover from the insult faster than the old animals, most likely due to presence of stronger antioxidant defense mechanisms in the former.

HNE, a by-product of lipid peroxidation, has been shown to accumulate in membranes at concentrations of 10 uM to 5 mM in response to oxidative insults (Esterbauer, Schaur et al. 1991; Uchida 2003). HNE is relatively stable and can transfer between subcellular compartments; thereby having the potential to interact with many different proteins within

the cell. It can react with the histidine, lysine and cysteine protein residues to generate stable adducts, resulting in alterations in the protein structure and function (Esterbauer, Schaur et al. 1991; Subramaniam, Roediger et al. 1997; Tamagno, Bardini et al. 2002; Uchida 2003). Here, we show that HNE directly modifies the γ-secretase component NCT in primary neurons. This finding is in agreement with a previous report showing that NCT is also modified by HNE in AD brain specimens (Gwon, Park et al. 2012). Modifications of the γ-secretase complex components, such as introducing mutations into PS1 (Berezovska, Lleo et al. 2005), Pen2 NT extension (Isoo, Sato et al. 2007; Uemura, Lill et al. 2009), or expressing different Aph1 isoforms (Serneels, Van Biervliet et al. 2009), have been shown to affect the conformation of PS1/γ-secretase and hence, the Aβ species generated. Now we propose that covalent modifications of NCT by the product of lipid peroxidation HNE, can also trigger similar pathogenic conformational changes.

We have also recently reported that peroxinitrite, an oxidant that accumulates during aging, induces PS1 conformational changes in cells *in vitro*, resulting in changes in the Aβ42/40 ratio (Guix, Wahle et al. 2012). Together, these data suggest that the effect of oxidative stress on PS1/γ-secretase might be a common pathogenic outcome, rather than being limited to a specific oxidation product (e.g. HNE) or specific reactive oxygen species.

HNE adducts are known to alter the activity of a variety of enzymes (reviewed in (Tamagno, Bardini et al. 2002; Uchida 2003)). Indeed, we found that HNE modified the activity of both β- and γ-secretase. Unlike the study of Gwon et al. (Gwon, Park et al. 2012), however, we found that HNE significantly impaired γ-secretase activity both in a cellular environment and in a cell free assay by causing structural change of the γ-secretase complex similar to that of FAD PS1 mutations. It is believed that FAD mutations in PS1 as well as pathogenic changes in PS1/γ -secretase in sporadic AD, may lead to a partial loss of function (Wang, Tang et al. 2006; De Strooper 2007; Shen and Kelleher 2007; Kelleher and Shen 2010; Xia, Watanabe et al. 2015). Indeed, many FAD PS1 mutations result in reduced overall Aβ production, however the ratio of the longer Aβ42 and Aβ43 species to Aβ40/total is steadily increased (Wang, Tang et al. 2006; De Strooper 2007; Shen and Kelleher 2007; Kelleher and Shen 2010; Xia, Watanabe et al. 2015).

On the other hand, the activity of β-secretase was intensified by HNE adducts covalently linked to the BACE protein in primary neurons. To the best of our knowledge, this is the first time that the HNE adducts are detected on the β-secretase enzyme, providing a molecular mechanism by which oxidative stress may affect BACE activity. This finding is consistent with previous studies showing that $H_2O_2/FeSO_4$ induced oxidative stress and generation of HNE increases β-secretase activity in NT_2 cells (Gwon, Park et al. 2012). We did not observe any significant change in the BACE levels within three hours of treatment of primary neurons with HNE; although studies by Tamagno et al.(Tamagno, Bardini et al. 2002; Tamagno, Parola et al. 2005) reported an increase in the BACE levels in NT_2 cells *in vitro* after 1 hr of HNE treatment. It is worth mentioning that in our experimental conditions HNE did not modify APP or C99 fragment (Supplementary Fig. 3) or any of the other components in the γ-secretase complex apart from NCT (Fig. 5), hence ruling out an extensive non-specific effect of HNE.

Although DTDP significantly altered Aβ levels in the mouse brain *in vivo*, it did not have any significant effect on either γ-secretase or BACE activity in cells or cell-free assay *in vitro*. Since increased GFAP immunoreactivity was detected in DTDP treated hemispheres within 6h of perfusion, it is plausible that astrocyte activation may mediate the DTDP effect on Aβ in the brain. Indeed, a number of studies reported a role of astrocytes in elevating Aβ levels (Mark, Lovell et al. 1997; Tamagno, Parola et al. 2005; Wang, Tang et al. 2006; Shen and Kelleher 2007; Kelleher and Shen 2010). It is also feasible that DTDP alters Aβ clearance, which would explain the increase in Aβ levels observed *in vivo* but not *in vitro*. Different clearance rates for Aβ40 versus Aβ42 could also explain an altered Aβ42/40 ratio.

Taken together, our results suggest a model (Fig. 9) in which HNE resulting from increased lipid peroxidation (due to aging, decreased antioxidant defenses, inflammation processes, etc.) covalently attaches and modifies both γ-secretase and BACE. These modifications differentially affect their activity, causing an increase in BACE activity but on the other hand, inflict γ-secretase conformational changes leading to decreased activity. Therefore, the total Aβ levels in the brain may not be significantly altered because of a “bottle-neck” effect, i.e. increased β-secretase but decreased γ-secretase activities. In addition, oxidative stress induced impairment of the Aβ clearance/degradation in the brain may somewhat hide PS1/γ-secretase loss-of-activity phenomena. However, the γ-secretase cleavage site on APP is altered as a consequence of NCT subunit modification by the HNE adducts, or as previously reported by nitrotyrosination of PS1 (Guix, Wahle et al. 2012), causing compression of the complex (detected as “closed” PS1 conformation) and partial loss of its activity. In accord with the step-wise cleavage model (Chavez-Gutierrez, Bammens et al. 2012), less active γ-secretase stops at producing longer Aβ species, resulting in higher $A\beta_4$2/40 ratio. This is also in agreement with the hypothesis of qualitative rather than quantitative shifts in the Aβ profiles representing pathogenic effect of all FAD mutations (Chavez-Gutierrez, Bammens et al. 2012). Altered ratio of longer Aβ species (Aβ42/43) to shorter (Aβ40) rather than total Aβ is associated with increased neurotoxicity and amyloid deposition. In turn, Aβ itself can induce oxidative stress/membrane lipid peroxidation and HNE production in neurons (Mark, Lovell et al. 1997; Mark, Pang et al. 1997). Thus, an initial local oxidative insult may initiate a feed-forward loop triggering and/or worsening amyloid pathology, creating a vicious cycle.

In conclusion, our study demonstrates a direct causative relationship between oxidative stress and lipid peroxidation, changes in conformation of PS1/γ-secretase and amyloid pathology, and proposes a molecular mechanism by which the lipid peroxidation product, HNE, affects the generation of toxic $A\beta_{42}$ species.

Supplementary Material

Refer to Web version on PubMed Central for supplementary material.

Acknowledgments

We would like to thank Dr. Alberto Serrano-Pozo, MD,PhD, for helpful discussions. This work was supported by National Institutes of Health grants [AG044486 and AG15379 to O.B.]; funding from BrightFocus foundation [O.B.], and the MGH ECOR Postdoctoral Fellowship Award [Fund for Medical Discovery to M.A.].

Abbreviations

Aβ	amyloid beta
DTDP	4,4'-dithiodipyridine
HNE	4-hydroxynonenal
E_{FRET}	Fluorescence Resonance Energy Transfer efficiency
FLIM	Fluorescence Lifetime Imaging Microscopy
NACA	N-acetylcysteine amide
PS1	presenilin 1

References

Atamna H, Boyle K. Amyloid-beta peptide binds with heme to form a peroxidase: relationship to the cytopathologies of Alzheimer's disease. Proc Natl Acad Sci U S A. 2006; 103(9):3381–3386. [PubMed: 16492752]

Berezovska O, Frosch M, et al. The Alzheimer-related gene presenilin 1 facilitates notch 1 in primary mammalian neurons. Brain Res Mol Brain Res. 1999; 69(2):273–280. [PubMed: 10366748]

Berezovska O, Lleo A, et al. Familial Alzheimer's disease presenilin 1 mutations cause alterations in the conformation of presenilin and interactions with amyloid precursor protein. J Neurosci. 2005; 25(11):3009–3017. [PubMed: 15772361]

Bergmans BA, De Strooper B. gamma-secretases: from cell biology to therapeutic strategies. Lancet Neurol. 2010; 9(2):215–226. [PubMed: 20129170]

Borchelt DR, Thinakaran G, et al. Familial Alzheimer's disease-linked presenilin 1 variants elevate Abeta1-42/1-40 ratio in vitro and in vivo. Neuron. 1996; 17(5):1005–1013. [PubMed: 8938131]

Butterfield DA. Amyloid beta-peptide (1–42)-induced oxidative stress and neurotoxicity: implications for neurodegeneration in Alzheimer's disease brain. A review. Free Radic Res. 2002; 36(12):1307–1313. [PubMed: 12607822]

Butterfield DA, Griffin S, et al. Amyloid beta-peptide and amyloid pathology are central to the oxidative stress and inflammatory cascades under which Alzheimer's disease brain exists. J Alzheimers Dis. 2002; 4(3):193–201. [PubMed: 12226538]

Butterfield DA, Hensley K, et al. Oxidatively induced structural alteration of glutamine synthetase assessed by analysis of spin label incorporation kinetics: relevance to Alzheimer's disease. J Neurochem. 1997; 68(6):2451–2457. [PubMed: 9166739]

Butterfield DA, Reed T, et al. Elevated protein-bound levels of the lipid peroxidation product, 4-hydroxy-2-nonenal, in brain from persons with mild cognitive impairment. Neurosci Lett. 2006; 397(3):170–173. [PubMed: 16413966]

Cai Z, Zhao B, et al. Oxidative stress and beta-amyloid protein in Alzheimer's disease. Neuromolecular Med. 2011; 13(4):223–250. [PubMed: 21901428]

Chavez-Gutierrez L, Bammens L, et al. The mechanism of gamma-Secretase dysfunction in familial Alzheimer disease. EMBO J. 2012; 31(10):2261–2274. [PubMed: 22505025]

Cirrito JR, May PC, et al. In vivo assessment of brain interstitial fluid with microdialysis reveals plaque-associated changes in amyloid-beta metabolism and half-life. J Neurosci. 2003; 23(26): 8844–8853. [PubMed: 14523085]

Cutler RG, Kelly J, et al. Involvement of oxidative stress-induced abnormalities in ceramide and cholesterol metabolism in brain aging and Alzheimer's disease. Proc Natl Acad Sci U S A. 2004; 101(7):2070–2075. [PubMed: 14970312]

De Strooper B. Loss-of-function presenilin mutations in Alzheimer disease. Talking Point on the role of presenilin mutations in Alzheimer disease. EMBO Rep. 2007; 8(2):141–146. [PubMed: 17268505]

Esterbauer H, Schaur RJ, et al. Chemistry and biochemistry of 4-hydroxynonenal, malonaldehyde and related aldehydes. Free Radic Biol Med. 1991; 11(1):81–128. [PubMed: 1937131]

Finkel T, Holbrook NJ. Oxidants, oxidative stress and the biology of ageing. Nature. 2000; 408(6809): 239–247. [PubMed: 11089981]

Garcia-Alloza M, Dodwell SA, et al. Plaque-derived oxidative stress mediates distorted neurite trajectories in the Alzheimer mouse model. J Neuropathol Exp Neurol. 2006; 65(11):1082–1089. [PubMed: 17086105]

Guix FX, Wahle T, et al. Modification of gamma-secretase by nitrosative stress links neuronal ageing to sporadic Alzheimer's disease. EMBO Mol Med. 2012; 4(7):660–673. [PubMed: 22488900]

Gwon AR, Park JS, et al. Oxidative lipid modification of nicastrin enhances amyloidogenic gamma-secretase activity in Alzheimer's disease. Aging Cell. 2012; 11(4):559–568. [PubMed: 22404891]

Hardy J, Selkoe DJ. The amyloid hypothesis of Alzheimer's disease: progress and problems on the road to therapeutics. Science. 2002; 297(5580):353–356. [PubMed: 12130773]

Harris ME, Hensley K, et al. Direct evidence of oxidative injury produced by the Alzheimer's beta-amyloid peptide (1–40) in cultured hippocampal neurons. Exp Neurol. 1995; 131(2):193–202. [PubMed: 7895820]

Isoo N, Sato C, et al. Abeta42 overproduction associated with structural changes in the catalytic pore of gamma-secretase: common effects of Pen-2 N-terminal elongation and fenofibrate. J Biol Chem. 2007; 282(17):12388–12396. [PubMed: 17329245]

Kelleher RJ 3rd, Shen J. Genetics. Gamma-secretase and human disease. Science. 2010; 330(6007): 1055–1056. [PubMed: 21097925]

Krstic D, Knuesel I. Deciphering the mechanism underlying late-onset Alzheimer disease. Nat Rev Neurol. 2013; 9(1):25–34. [PubMed: 23183882]

Kuperstein I, Broersen K, et al. Neurotoxicity of Alzheimer's disease Abeta peptides is induced by small changes in the Abeta42 to Abeta40 ratio. EMBO J. 2010; 29(19):3408–3420. [PubMed: 20818335]

Lewczuk P, Esselmann H, et al. Neurochemical diagnosis of Alzheimer's dementia by CSF Abeta42, Abeta42/Abeta40 ratio and total tau. Neurobiol Aging. 2004; 25(3):273–281. [PubMed: 15123331]

Lleo A, Berezovska O, et al. Nonsteroidal anti-inflammatory drugs lower Abeta42 and change presenilin 1 conformation. Nat Med. 2004; 10(10):1065–1066. [PubMed: 15448688]

Lovell MA, Markesbery WR. Ratio of 8-hydroxyguanine in intact DNA to free 8-hydroxyguanine is increased in Alzheimer disease ventricular cerebrospinal fluid. Arch Neurol. 2001; 58(3):392–396. [PubMed: 11255442]

Mangialasche F, Polidori MC, et al. Biomarkers of oxidative and nitrosative damage in Alzheimer's disease and mild cognitive impairment. Ageing Res Rev. 2009; 8(4):285–305. [PubMed: 19376275]

Mark RJ, Lovell MA, et al. A role for 4-hydroxynonenal, an aldehydic product of lipid peroxidation, in disruption of ion homeostasis and neuronal death induced by amyloid beta-peptide. J Neurochem. 1997; 68(1):255–264. [PubMed: 8978733]

Mark RJ, Pang Z, et al. Amyloid beta-peptide impairs glucose transport in hippocampal and cortical neurons: involvement of membrane lipid peroxidation. J Neurosci. 1997; 17(3):1046–1054. [PubMed: 8994059]

McLellan ME, Kajdasz ST, et al. In vivo imaging of reactive oxygen species specifically associated with thioflavine S-positive amyloid plaques by multiphoton microscopy. J Neurosci. 2003; 23(6): 2212–2217. [PubMed: 12657680]

Nemoto S, Takeda K, et al. Role for mitochondrial oxidants as regulators of cellular metabolism. Mol Cell Biol. 2000; 20(19):7311–7318. [PubMed: 10982848]

Nishikawa T, Edelstein D, et al. Normalizing mitochondrial superoxide production blocks three pathways of hyperglycaemic damage. Nature. 2000; 404(6779):787–790. [PubMed: 10783895]

Pratico D, Uryu K, et al. Increased lipid peroxidation precedes amyloid plaque formation in an animal model of Alzheimer amyloidosis. The Journal of neuroscience : the official journal of the Society for Neuroscience. 2001; 21(12):4183–4187. [PubMed: 11404403]

Reed TT, Pierce WM Jr, et al. Proteomic identification of nitrated brain proteins in early Alzheimer's disease inferior parietal lobule. J Cell Mol Med. 2009; 13(8):2019–2029. [PubMed: 18752637]

Reed TT, Pierce WM, et al. Proteomic identification of HNE-bound proteins in early Alzheimer disease: Insights into the role of lipid peroxidation in the progression of AD. Brain Res. 2009; 1274:66–76. [PubMed: 19374891]

Sajdel-Sulkowska EM, Marotta CA. Alzheimer's disease brain: alterations in RNA levels and in a ribonuclease-inhibitor complex. Science. 1984; 225(4665):947–949. [PubMed: 6206567]

Sayre LM, Zelasko DA, et al. 4-Hydroxynonenal-derived advanced lipid peroxidation end products are increased in Alzheimer's disease. J Neurochem. 1997; 68(5):2092–2097. [PubMed: 9109537]

Serneels L, Van Biervliet J, et al. gamma-Secretase heterogeneity in the Aph1 subunit: relevance for Alzheimer's disease. Science. 2009; 324(5927):639–642. [PubMed: 19299585]

Shen J, Kelleher RJ 3rd. The presenilin hypothesis of Alzheimer's disease: evidence for a loss-of-function pathogenic mechanism. Proc Natl Acad Sci U S A. 2007; 104(2):403–409. [PubMed: 17197420]

Shichiri M, Yoshida Y, et al. alpha-Tocopherol suppresses lipid peroxidation and behavioral and cognitive impairments in the Ts65Dn mouse model of Down syndrome. Free Radic Biol Med. 2011; 50(12):1801–1811. [PubMed: 21447382]

Subramaniam R, Roediger F, et al. The lipid peroxidation product, 4-hydroxy-2-trans-nonenal, alters the conformation of cortical synaptosomal membrane proteins. J Neurochem. 1997; 69(3):1161–1169. [PubMed: 9282939]

Subramanian R, Tam J, et al. Novel cytochrome p450 bioactivation of a terminal phenyl acetylene group: formation of a one-carbon loss benzaldehyde and other oxidative products in the presence of N-acetyl cysteine or glutathione. Chem Res Toxicol. 2011; 24(5):677–686. [PubMed: 21395287]

Sultana R, Butterfield DA. Role of oxidative stress in the progression of Alzheimer's disease. Journal of Alzheimer's disease : JAD. 2010; 19(1):341–353.

Sun SY. N-acetylcysteine, reactive oxygen species and beyond. Cancer Biol Ther. 2010; 9(2):109–110. [PubMed: 19949311]

Takeda S, Sato N, et al. Novel microdialysis method to assess neuropeptides and large molecules in free-moving mouse. Neuroscience. 2011; 186:110–119. [PubMed: 21530615]

Tamagno E, Bardini P, et al. Oxidative stress increases expression and activity of BACE in NT2 neurons. Neurobiol Dis. 2002; 10(3):279–288. [PubMed: 12270690]

Tamagno E, Parola M, et al. Beta-site APP cleaving enzyme up-regulation induced by 4-hydroxynonenal is mediated by stress-activated protein kinases pathways. J Neurochem. 2005; 92(3):628–636. [PubMed: 15659232]

Uchida K. 4-Hydroxy-2-nonenal: a product and mediator of oxidative stress. Prog Lipid Res. 2003; 42(4):318–343. [PubMed: 12689622]

Uemura K, Farner KC, et al. Substrate docking to gamma-secretase allows access of gamma-secretase modulators to an allosteric site. Nat Commun. 2010; 1:130. [PubMed: 21119643]

Uemura K, Lill CM, et al. Allosteric modulation of PS1/gamma-secretase conformation correlates with amyloid beta(42/40) ratio. PLoS One. 2009; 4(11):e7893. [PubMed: 19924286]

Wahlster L, Arimon M, et al. Presenilin-1 adopts pathogenic conformation in normal aging and in sporadic Alzheimer's disease. Acta Neuropathol. 2013; 125(2):187–199. [PubMed: 23138650]

Wang R, Tang P, et al. Regulation of tyrosinase trafficking and processing by presenilins: partial loss of function by familial Alzheimer's disease mutation. Proc Natl Acad Sci U S A. 2006; 103(2): 353–358. [PubMed: 16384915]

Williams TI, Lynn BC, et al. Increased levels of 4-hydroxynonenal and acrolein, neurotoxic markers of lipid peroxidation, in the brain in Mild Cognitive Impairment and early Alzheimer's disease. Neurobiol Aging. 2006; 27(8):1094–1099. [PubMed: 15993986]

Wiltfang J, Esselmann H, et al. Amyloid beta peptide ratio 42/40 but not A beta 42 correlates with phospho-Tau in patients with low- and high-CSF A beta 40 load. J Neurochem. 2007; 101(4): 1053–1059. [PubMed: 17254013]

Wolfe MS. When loss is gain: reduced presenilin proteolytic function leads to increased Abeta42/Abeta40. Talking Point on the role of presenilin mutations in Alzheimer disease. EMBO Rep. 2007; 8(2):136–140. [PubMed: 17268504]

Xia D, Watanabe H, et al. Presenilin-1 knockin mice reveal loss-of-function mechanism for familial Alzheimer's disease. Neuron. 2015; 85(5):967–981. [PubMed: 25741723]

Xie H, Hou S, et al. Rapid cell death is preceded by amyloid plaque-mediated oxidative stress. Proc Natl Acad Sci U S A. 2013

Highlights

- Lipid peroxidation product HNE and oxidant DTDP increase Aβ42/40 ratio *in vivo*
- Oxidative stress/HNE induce FAD-like pathogenic conformation of PS1/γ-secretase
- HNE-adducts on Nct and BACE reduce and enhance secretase activities, respectively
- HNE may initiate a pathologic cascade by selectively increasing Aβ42 levels

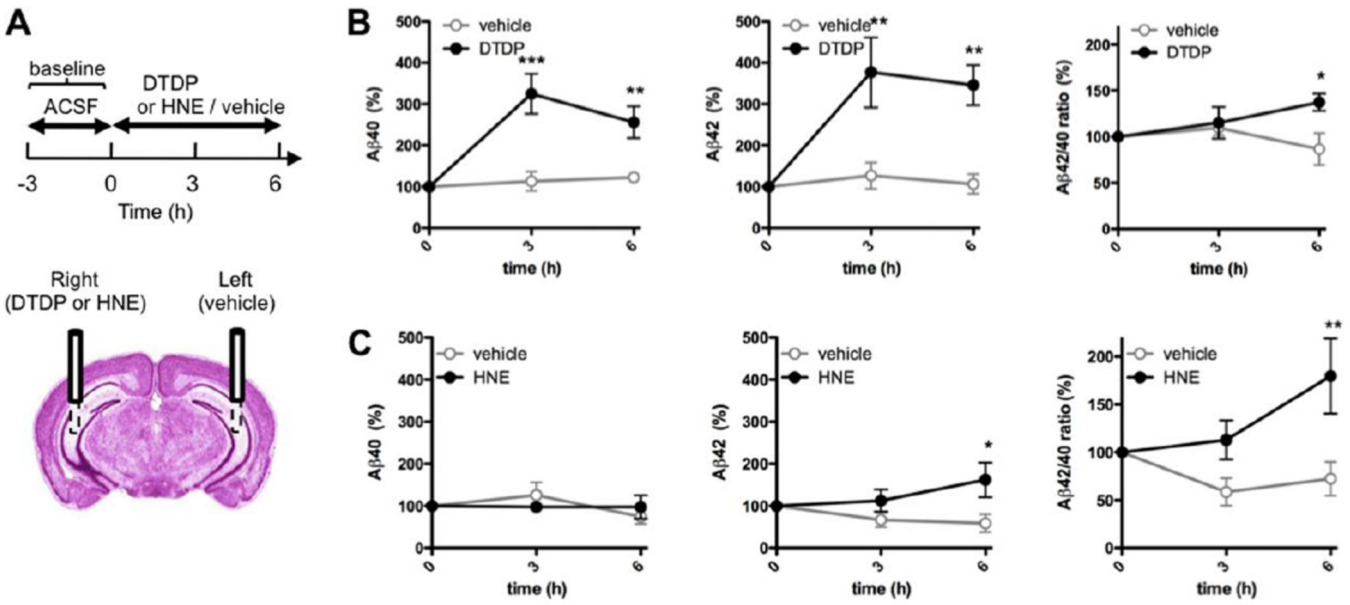

Fig. 1. Locally induced oxidative stress *in vivo* alters Aβ levels in wild-type mice

(A) Scheme of the time frame for DTDP, HNE or vehicle treatments delivered via microdialysis probe into hippocampus of 12 months old mice. (B–C) Levels of Aβ40 and Aβ42 in the ISF and the Aβ42/40 ratio after DTDP (B) or HNE (C) treatment were compared to that in the vehicle trated hemisphere of the same mouse (n = 5 animals). The baseline levels of ISF Aβ40 and Aβ42 collected prior to the treatment were 15.61 ± 1.35 pM and 6.31 ± 0.62 pM, respectively. Data represent the mean ± SEM, presented as percentage values relative to the time point zero of each hemisphere. Two-way ANOVA, Bonferroni posttest. *$p < 0.05$, **$p < 0.01$, ***$p < 0.001$, compared to the same time point of the vehicle-treated hemisphere.

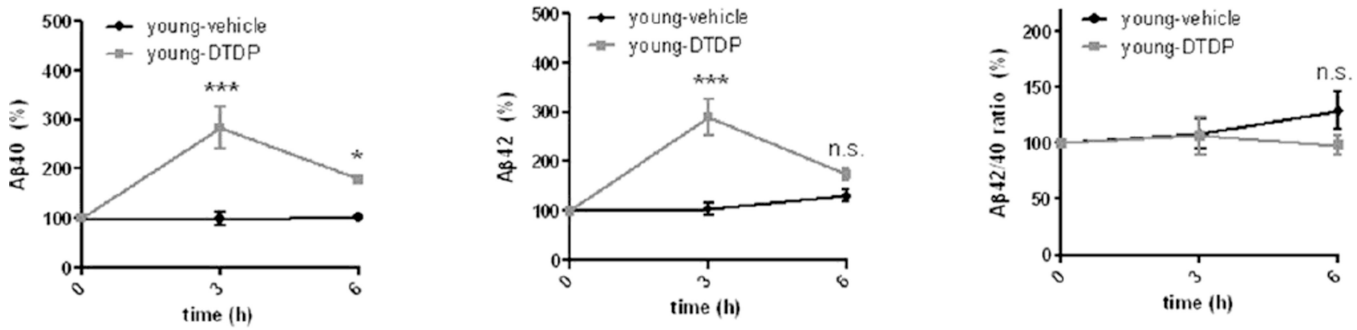

Fig. 2. Response to acute oxidative stress in young wild-type mice

ISF Aβ40, Aβ42 levels and the Aβ42/40 ratio after DTDP treatment delivered via the microdialysis probe to the brain of young (4 months old) wild-type mice (n = 3–4 animals). The baseline levels of ISF Aβ40 and Aβ42 at the time point zero were 15.28 ± 1.19 pM and 4.68 ± 0.70 pM, respectively. Data represent the mean ± SEM, presented as percentage values relative to the time point zero of each hemisphere. Two-way ANOVA, Bonferroni posttest. *$p < 0.05$, **$p < 0.01$, ***$p < 0.001$, compared to the same time point of the vehicle-treated hemisphere.

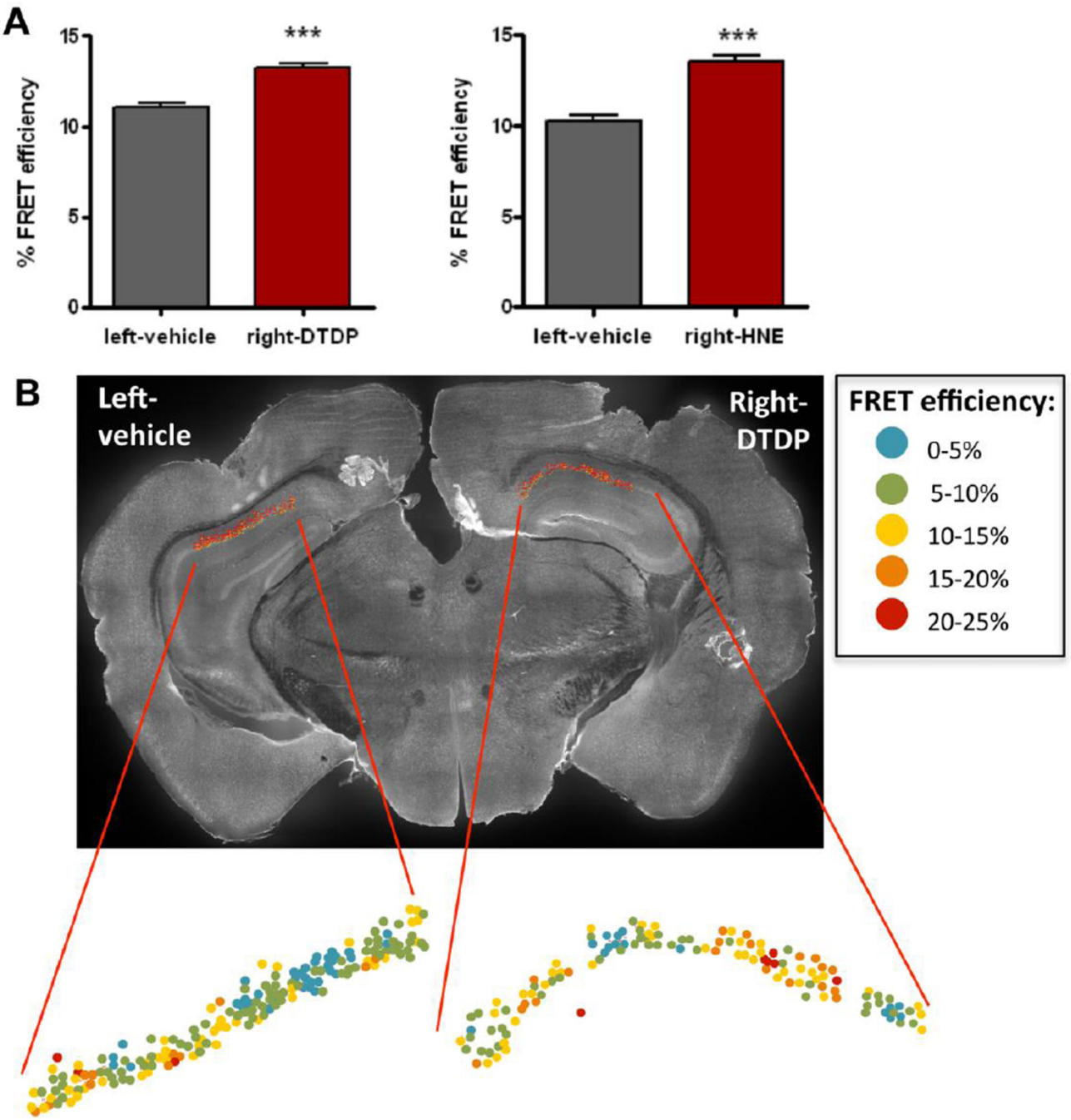

Fig. 3. Locally induced oxidative stress *in vivo* alters PS1 conformation

PS1 conformation in neurons of the CA1 area of hippocampus was assessed by FLIM analysis 6h after the treatment with DTDP or HNE by microdialysis. (A) FRET efficiency (%) values representing proximity between PS1 NT and CT in neurons, treated with vehicle control (left hemisphere) or DTDP/HNE (right hemisphere). Data represent the mean ± SEM of at least three different brains. T-test nonparametric: Mann Whitney test. ***$p < 0.001$, compared to vehicle-treated hemisphere. (B) Representative image of a brain section immunostained with PS1-NT and -CT antibodies after DTDP treatment by microdialysis.

Map of the distribution of neurons within CA1 area shows color-coded $\%E_{FRET}$ values as determined by FLIM analysis.

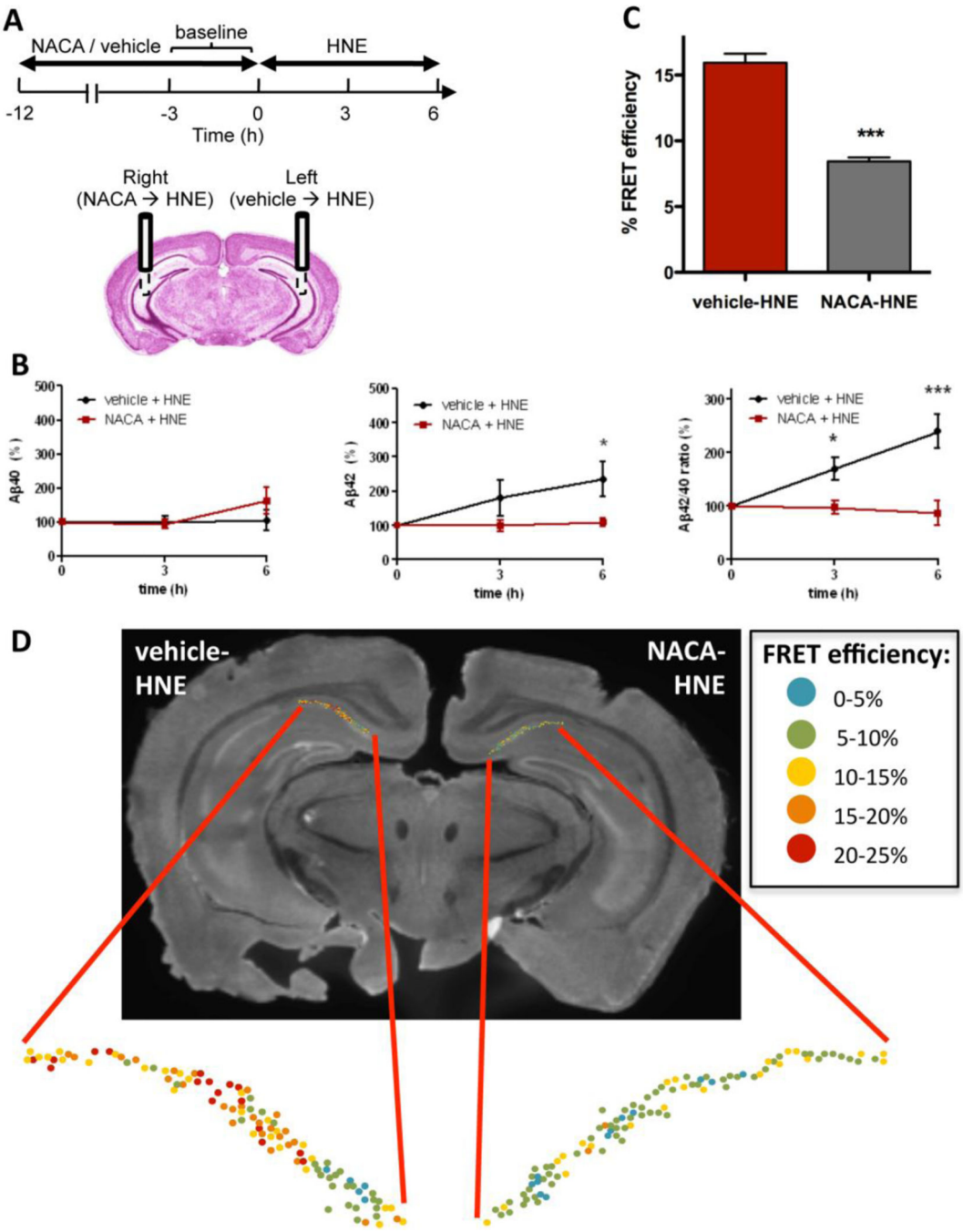

Fig. 4. Antioxidant NACA pretreatment precludes HNE effect on Aβ and PS1 conformation

(A) Scheme of the experiment with NACA/vehicle pretreatment prior to the HNE delivery. (B) Levels of Aβ40 and Aβ42 in the ISF and the Aβ42/40 ratio after vehicle-HNE and NACA-HNE treatment (n = 4–5 animals). (C) FRET efficiency (%) values in neurons of the vehicle-HNE treated (left) or NACA-HNE (right) hemispheres. Data represent the mean ± SEM. T-test nonparametric: Mann Whitney test. *p < 0.05, ***p < 0.001, compared to vehicle-treated hemisphere; n=3 brains. (D) Representative image of a brain section immunostained with PS1 -NT and -CT antibodies after vehicle-HNE and NACA-HNE

treatment by microdialysis. Map of the distribution of neurons within hippocampal CA1 area shows color-coded $\%E_{FRET}$ values as determined by FLIM analysis.

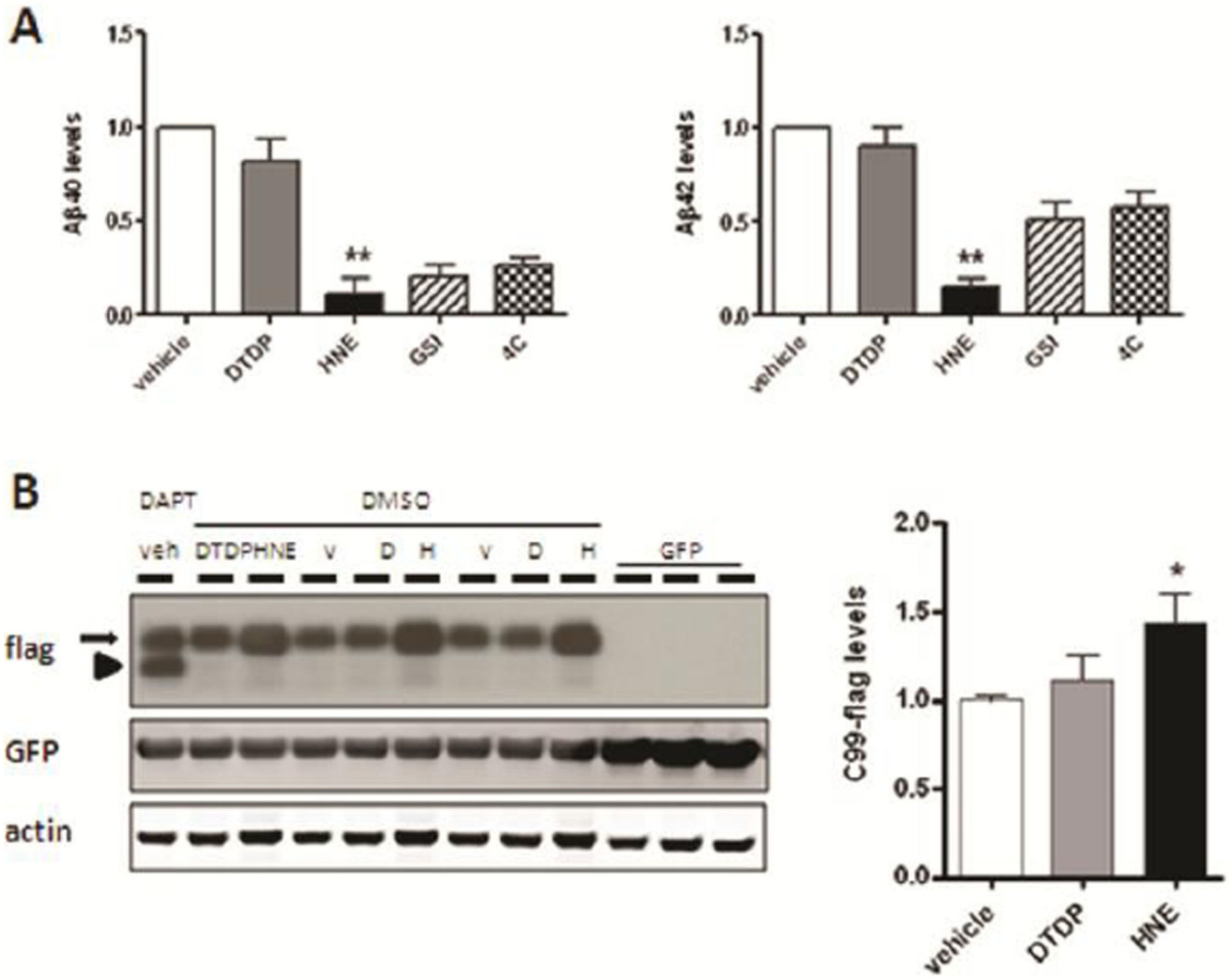

Fig. 5. Effect of DTDP and HNE on γ-secretase

(A) Cell-free γ-secretase activity assay. Membrane-enriched fractions extracted from wild-type mouse brains were incubated with the substrate C100-flag and treated with vehicle, DTDP (100 uM) or HNE (1 mM). Treatment with the γ-secretase inhibitor L-685,458 (50 nM) or incubation at 4°C were used as negative controls. Aβ40 and Aβ42 levels are shown as values relative to the vehicle treatment. Data represent the mean ± SEM of five independent experiments. T-test: *$p < 0.05$, **$p < 0.01$, compared to vehicle treatment. (B) HEK293 cells co-transfected with C99-flag and GFP plasmids were treated with vehicle, DTDP or HNE. The levels of C99-flag (arrow) were quantified and normalized to GFP (transfection efficiency) and to actin (loading control). C83-flag fragment is shown by an arrowhead. Data represent the mean ± SEM (relative to vehicle) of four independent experiments performed in triplicate. T-test: *$p < 0.05$, compared to vehicle treatment.

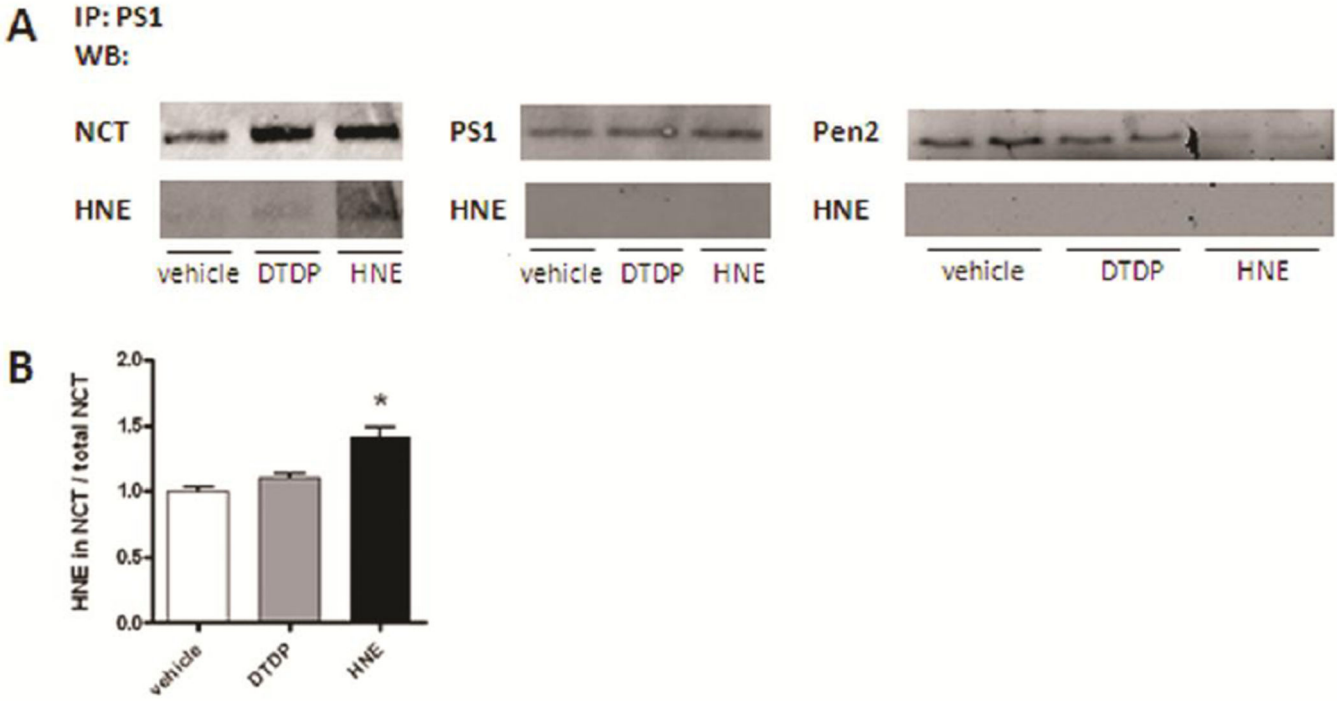

Fig. 6. HNE covalently modifies nicastrin

γ-secretase complexes were immunoprecipitated from primary neurons treated with vehicle, DTDP or HNE using PS1-NT and PS1-loop antibodies. (A) Immunoblots were simultaneously probed with the corresponding antibodies to NCT, PS1 and Pen2, and with an antibody specific to HNE adducts. The Li-Cor Odyssey infrared imaging system was used to detect HNE adducts on exactly the same bands of NCT, PS1 and Pen2, respectively. (B) The HNE levels were normalized to the immunoprecipitated NCT levels. There was no detectable HNE signal on PS1 and Pen2 bands. Data represent the mean ± SEM (relative to vehicle) of three independent experiments. T-test: *$p < 0.05$, compared to vehicle treatment.

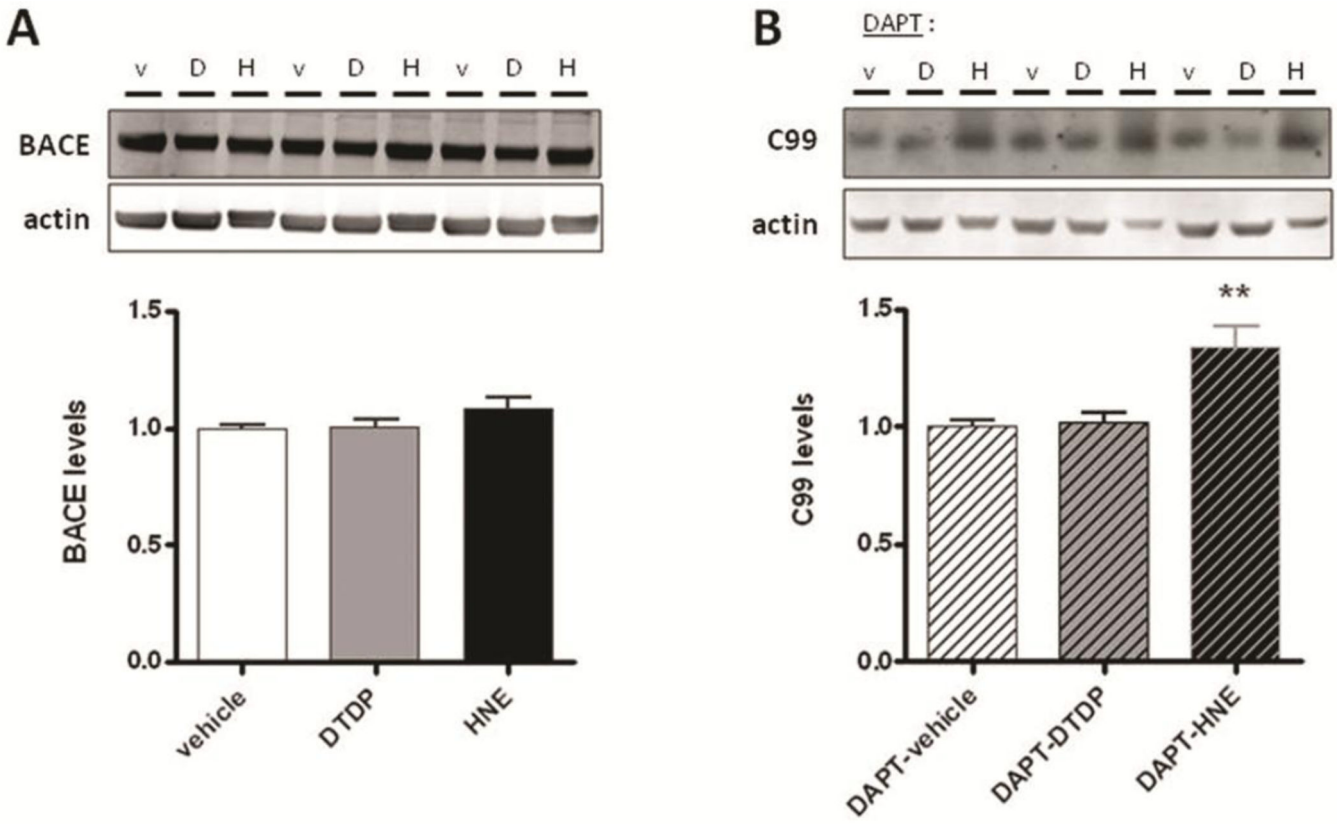

Fig. 7. Effect of DTDP and HNE on BACE

(A) Western blot analysis of BACE protein levels in primary neurons after DTDP or HNE treatment. (b) Primary neurons were pre-treated overnight with DAPT before incubation with DTDP or HNE, and the ammount of APP C99 fragments was quantified by a C99 specific antibody. Data represent the mean ± SEM (relative to vehicle) of three independent experiments performed at least in triplicates. T-test: **$p < 0.01$, compared to vehicle treatment.

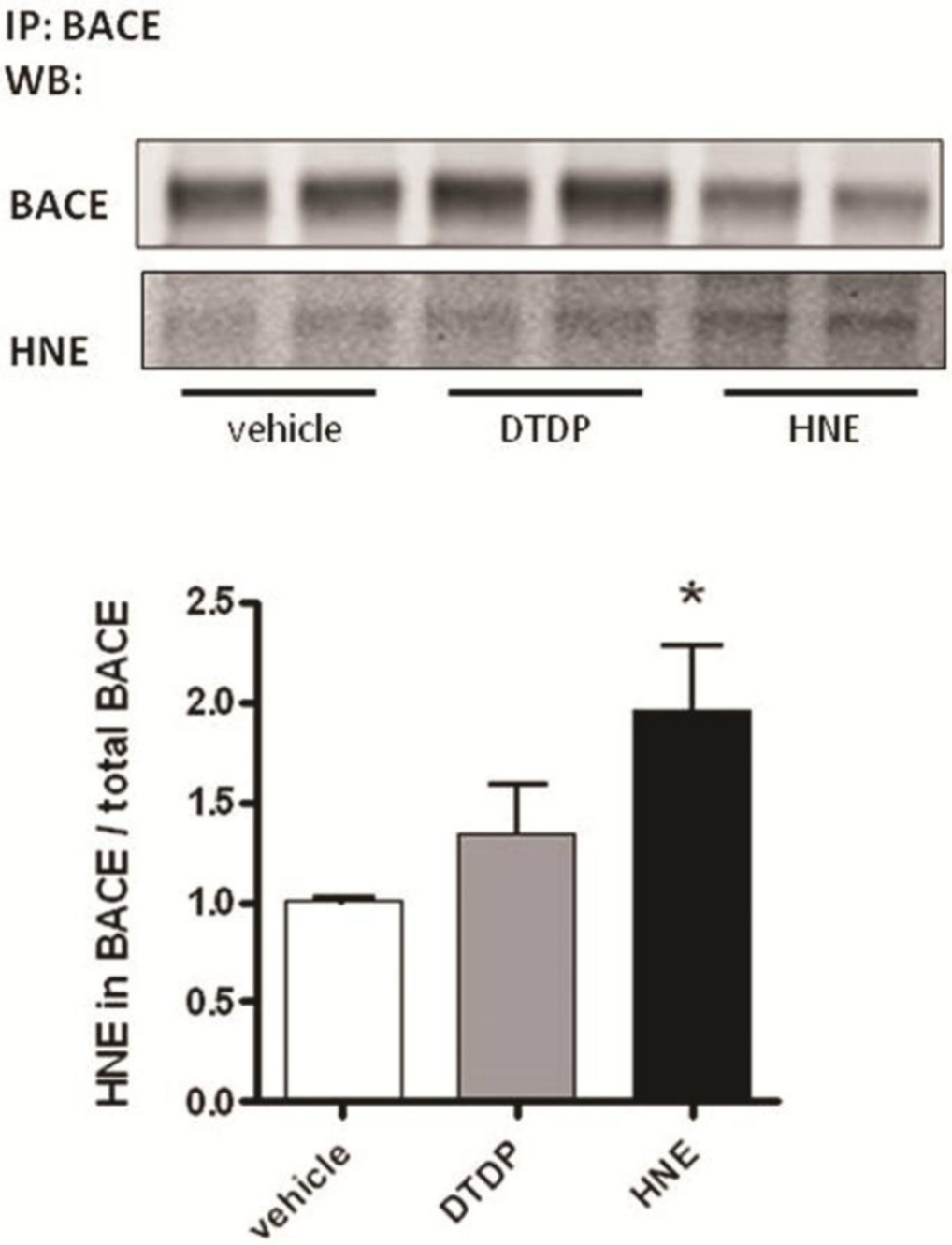

Fig. 8. HNE covalently modifies BACE

BACE was immunoprecipitated from primary neurons treated with DTDP or HNE. Immunoblots were simultaneously probed with antibodies specific to BACE and to HNE adducts, using the Li-Cor Odyssey infrared imaging system. The HNE levels were normalized to the immunoprecipitated BACE levels. Data represent the mean ± SEM (relative to vehicle) of four independent experiments. T-test: *$p < 0.05$, compared to vehicle treatment.

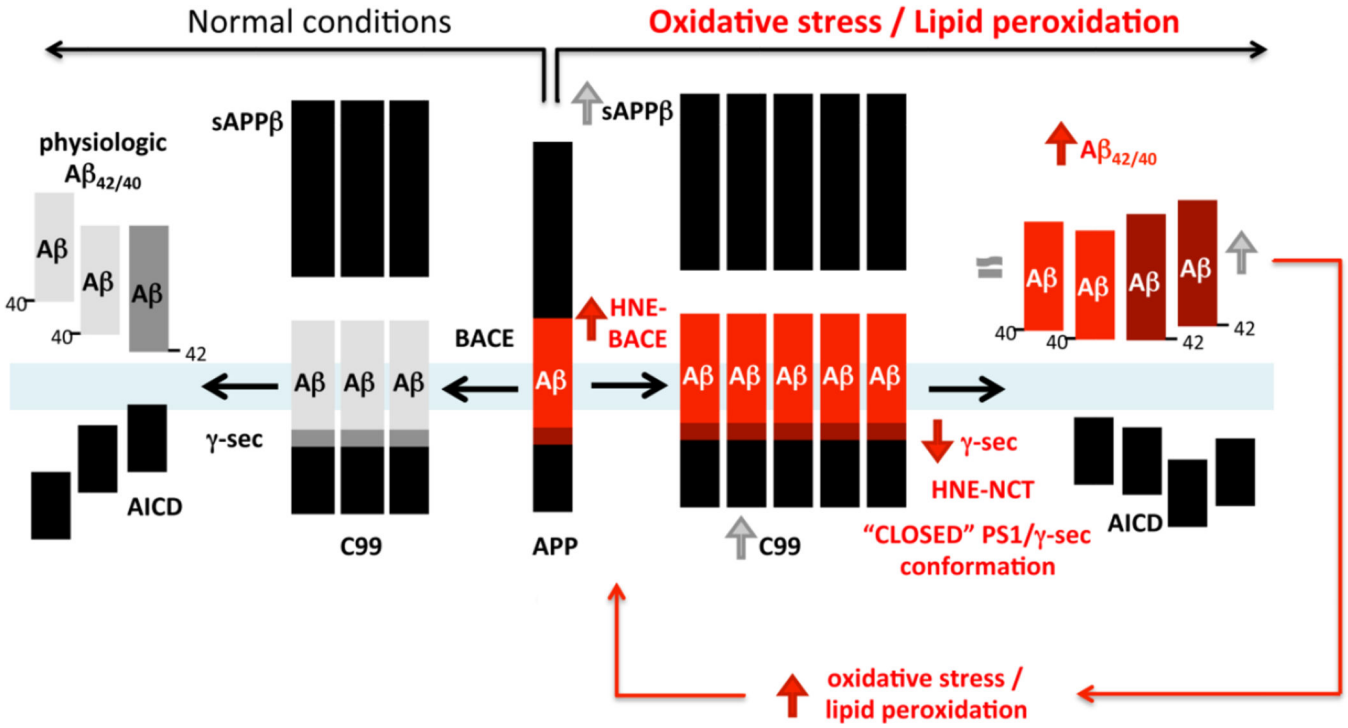

Fig. 9. Schematic representation of the effect of HNE on Aβ production

We propose that HNE resulting from lipid peroxidation covalently modifies both BACE and nicastrin/γ-secretase. As a result, β-secretase activity is enhanced, whereas γ-secretase activity is decreased. Therefore, the total Aβ levels in the brain may not significantly change due to this "bottle-neck" effect. At the same time, the HNE modification of NCT triggers a pathogenic change in PS1/γ-secretase conformation, similar to that of FAD PS1 mutations, resulting in increased Aβ42 generation and higher Aβ42/40 ratio.